

Brownian Motion In Dire Straits

D. Holcman¹, Z. Schuss²

Abstract

The passage of Brownian motion through a bottleneck in a bounded domain is a rare event and as the bottleneck radius shrinks to zero the mean time for such passage increases indefinitely. Its calculation reveals the effect of geometry and smoothness on the flux through the bottleneck. We find new behavior of the narrow escape time through bottlenecks in planar and spatial domains and on a surface. Some applications in cellular biology and neurobiology are discussed.

1 Introduction

The narrow escape problem is to calculate the mean first passage time (MFPT) of Brownian motion from a domain with mostly reflecting boundary to a small absorbing window. The MFPT, also known as the narrow escape time (NET), was calculated in [1]-[12] for small absorbing windows in a smooth reflecting boundary. Several more complex cases were considered in [6]-[8], such as the NET through a window at a corner or at a cusp in the boundary and the NET on Riemannian manifolds. The calculation of the NET in composite domains with long necks, as shown in Figure 1, was attempted in [12] and [13] and ultimately accomplished in [14]. The NET problem in a planar domain with an absorbing window at the end of a funnel was considered in [15]. The case of planar domains that consist of large compartments interconnected by funnel-shaped bottlenecks was also considered in [15].

In this paper we consider Brownian motion in two- and three-dimensional domains whose boundaries are smooth and reflecting, except for a small absorbing window at the end of a cusp-shaped funnel, as shown in Figure 2. The cusp can be formed by a partial block of a planar domain, as shown in Figure 3. The NET from this type of a domain was calculated in [15] only for the planar case.

The results of [1]-[12] for small absorbing windows in a smooth reflecting boundary of a domain Ω can be summarized as follows. In the two-dimensional case considered in [7] the absorbing boundary $\partial\Omega_a$ is a small window in the smooth boundary $\partial\Omega$ that is otherwise reflecting to Brownian trajectories. The MFPT from $\mathbf{x} \in \Omega$ to the absorbing boundary $\partial\Omega_a$, denoted $\bar{\tau}_{\mathbf{x} \rightarrow \partial\Omega_a}$, is the NET from the domain Ω to the small window $\partial\Omega_a$ (of length a), such that $\varepsilon = \pi|\partial\Omega_a|/|\partial\Omega| = \pi a/|\partial\Omega| \ll 1$ (this corrects the definition in [7]). Because the singularity of Neumann's function in the plane is logarithmic the MFPT is given by

$$\bar{\tau}_{\mathbf{x} \rightarrow \partial\Omega_a} = \frac{|\Omega|}{\pi D} \ln \frac{|\partial\Omega|}{\pi|\partial\Omega_a|} + O(1) \text{ for } \mathbf{x} \in \Omega \text{ outside a boundary layer near } \partial\Omega_a. \quad (1)$$

¹Department of Applied Mathematics, Tel-Aviv University, Tel-Aviv 69978, Israel. Department of Mathematics and Computational Biophysics, Ecole Normale Supérieure, 46 rue d'Ulm 75005 Paris, France. This research is supported by an ERC-starting-Grant.

²Department of Mathematics, Tel-Aviv University, Tel-Aviv 69978, Israel.

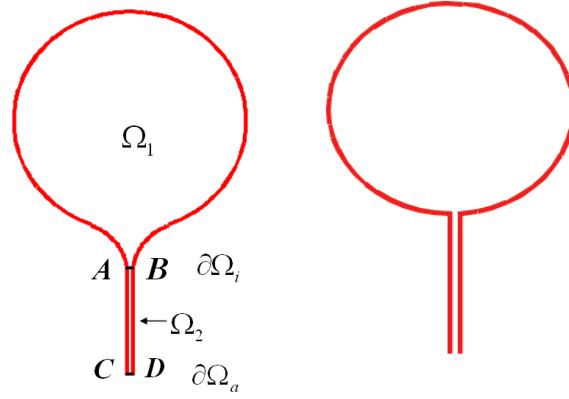


Figure 1: A mathematical idealization of a cross section of smooth and sharp connections approximating the spine morphology: **Left:** The cross section is a composite domain that consists of a bulky head Ω_1 connected smoothly by an interface $\partial\Omega_i = AB$ to a narrow neck Ω_2 . The entire boundary is $\partial\Omega_r$ (reflecting), except for a small absorbing part $\partial\Omega_a = CD$. **Right:** A cross section of a sharp connection.

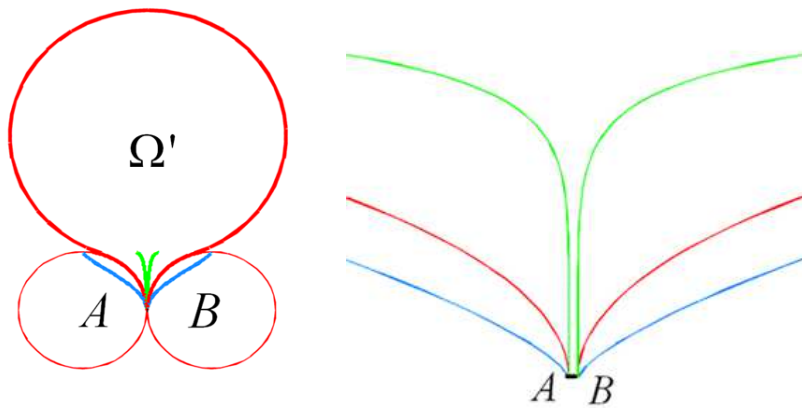


Figure 2: **Left:** The planar (dimensional) domain Ω' is bounded by a large circular arc connected smoothly to a funnel formed by moving ε apart two tangent circular arcs of radius R_c (i.e., $\overline{AB} = \varepsilon$). **Right:** Blowup of the cusp region. The red, green, and blue necks correspond to $\nu_{\pm} = 1, 0.4$, and 5 in (12), respectively.

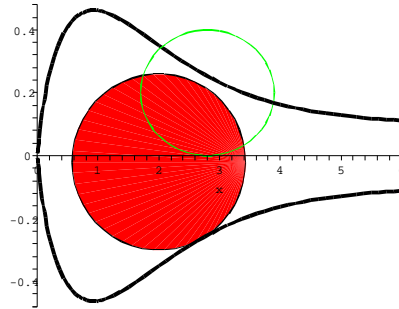


Figure 3: Narrow straits formed by a partial block (solid disk) of the passage from the head to the neck of the domain enclosed by the black line. Inside the green circle the narrow straits can be approximated by the gap between adjacent circles.



$$f(x) = \begin{cases} 0.3 + 0.5x & x < 2 \\ \sqrt{2.112500002 - (x - 2.65)^2} & x < 4.103444186 \end{cases}, 0 \leq x \leq 4.103444186,$$

Surface of revolution formed when
 ≤ 4.103444186 , is rotated about a horizontal axis.

Figure 4: Narrow straits formed by a cone-shaped funnel. Axes are rotated 90° about the y -axis.

In the three-dimensional case the MFPT to a circular absorbing window $\partial\Omega_a$ of small radius a centered at $\mathbf{0}$ on the boundary $\partial\Omega$ is given by [16]

$$\bar{\tau}_{\mathbf{x} \rightarrow \partial\Omega_a} = \frac{|\Omega|}{4aD \left[1 + \frac{L(\mathbf{0}) + N(\mathbf{0})}{2\pi} a \log a + o(a \log a) \right]}, \quad (2)$$

where $L(\mathbf{0})$ and $N(\mathbf{0})$ are the principal curvatures of the boundary at the center of $\partial\Omega_a$.

However, the MFPT from a domain to an absorbing interface located at the end of a funnel, as shown in Figure 2, cannot be calculated by the methods of [6]-[8], [16], because the contribution of the singular part of Neumann's function to the MFPT in a composite domain with a funnel or another bottleneck is not necessarily dominant. Also the method of matched asymptotic expansions, used in [1]-[3], [17] for calculating the MFPT to the interface on a smooth boundary, requires major modifications for an interface at the end of a bottleneck, because the boundary layer problem does not reduce to the classical electrified disk problem [19]. Altogether different boundary or internal layers at absorbing windows located at the end of a cusp-like funnel are needed. The methods used in [12] and [13] for constructing the MFPT in composite domains of the type shown in Figure 1(right) are made precise here and the new method extends to domains of the type shown in Figure 1(left).

The new results of this paper are as follows. In Section 2 we prove that the MFPT to the narrow straits formed by a partial block of a planar domain (see Figures 2 and 3) is given by

$$\bar{\tau} = \sqrt{\frac{R_c(R_c + r_c)}{2r_c\varepsilon}} \frac{\pi|\Omega|}{2D} (1 + o(1)) \quad \text{for } \varepsilon \ll |\partial\Omega|, R_c, r_c, \quad (3)$$

where R_c and r_c are the curvatures at the neck and ε is the width of the straits. More general cases are also considered. In Section 3 we prove that the MFPT in the solid of revolution obtained by rotating the symmetric domain Ω in Figure 2(left) about its axis of symmetry is given by

$$\bar{\tau} = \frac{1}{\sqrt{2}} \left(\frac{R_c}{a} \right)^{3/2} \frac{|\Omega|}{R_c D} (1 + o(1)) \quad \text{for } a \ll R_c, \quad (4)$$

where the radius of the cylindrical neck is $a = \varepsilon/2$. In Section 4 we consider Brownian motion on a surface of revolution generated by rotating the curve in Figure 2(left) about its axis of symmetry. We use the representation of the generating curve

$$y = r(x), \quad \Lambda < x < 0$$

where the x -axis is horizontal with $x = \Lambda$ at the absorbing end AB . We assume that the parts of the curve that generate the funnel have the form

$$\begin{aligned} r(x) &= O(\sqrt{|x|}) \quad \text{near } x = 0 \\ r(x) &= a + \frac{(x - \Lambda)^{1+\nu}}{\nu(1+\nu)\ell^\nu} (1 + o(1)) \quad \text{for } \nu > 0 \text{ near } x = \Lambda, \end{aligned} \quad (5)$$

where $a = \frac{1}{2}\overline{AB} = \varepsilon/2$ is the radius of the gap, and the constant ℓ has dimension of length. For $\nu = 1$ the parameter ℓ is the radius of curvature R_c at $x = \Lambda$. We prove that the MFPT from the head to the absorbing end AB is given by

$$\bar{\tau} \sim \frac{\mathcal{S}(\Lambda)}{2D} \frac{\left(\frac{\ell}{(1+\nu)a}\right)^{\nu/1+\nu} \nu^{1/1+\nu}}{\sin \frac{\nu\pi}{1+\nu}}, \quad (6)$$

where \mathcal{S} is the entire unscaled area of the surface. In particular, for $\nu = 1$ we get the MFPT

$$\bar{\tau} \sim \frac{\mathcal{S}}{4D\sqrt{a/2\ell}}. \quad (7)$$

The case $\nu = 0$ corresponds to an absorbing circular cap of small radius a on a closed surface. For a sphere we get the known result

$$\bar{\tau} = \frac{2R^2}{D} \log \frac{\sin \frac{\theta}{2}}{\sin \frac{\delta}{2}}, \quad (8)$$

where θ is the angle between \mathbf{x} and the south-north axis of the sphere and $a = R \sin \delta/2$ (see [8]–[11]).

If a right circular cylinder of a small radius a and length L is attached to the surface at $z = \Lambda$, the NET from the composite surface is given by

$$\bar{\tau} = \frac{\mathcal{S}(\Lambda)}{2D} \frac{\left(\frac{\ell}{(1+\nu)a}\right)^{\nu/1+\nu} \nu^{1/1+\nu}}{\sin \frac{\nu\pi}{1+\nu}} + \frac{\mathcal{S}L}{2\pi Da} + \frac{L^2}{2D} \text{ for } a \ll \ell \quad (9)$$

(see [14] for a different derivation). We also find the NET and the exit probability when there are N absorbing windows at the ends of narrow necks. These are related to the principal eigenvalue of the Laplacian in dumbbell-shaped domains that consists of heads interconnected by narrow necks, which, in turn, is related to the effective diffusion in such domains. In Section 5 we calculate the NET from composite domains that consist of a head connect by a funnel to a narrow cylindrical neck and calculate the principal eigenvalue composite and dumbbell-shaped domains. Finally, in Section 6 we calculate the mean time $\bar{\tau}$ for a Brownian needle to turn around in a tightly fitting planar strip. For a needle of length l_0 in a strip of width l it is given by

$$\bar{\tau} = \frac{\pi \left(\frac{\pi}{2} - 1\right)}{D_r \sqrt{l_0(l_0 - l)}} \sqrt{\frac{D_X}{D_r}} \left(1 + O\left(\sqrt{\frac{l_0 - l}{l_0}}\right)\right), \quad (10)$$

where D_r is the rotational diffusion coefficient and D_X is the translational diffusion coefficient along the needle. We close this article by providing several applications to cellular biology.

2 The MFPT to a bottleneck

We consider the NET problem in an asymmetric planar domain, as in Figure 3 or in an asymmetric version of the (dimensional) domain Ω' in Figure 2. We use the (dimensional) representation of the boundary curves

$$y' = r_{\pm}(x'), \quad \Lambda' < x' < 0 \text{ for the upper and lower parts, respectively} \quad (11)$$

where the x' -axis is horizontal with $x' = \Lambda'$ at AB . We assume that the parts of the curve that generate the funnel have the form

$$\begin{aligned} r_{\pm}(x') &= O(\sqrt{|x'|}) \text{ near } x' = 0 \\ r_{\pm}(x') &= \pm a' \pm \frac{(x' - \Lambda')^{1+\nu_{\pm}}}{\nu_{\pm}(1+\nu_{\pm})\ell_{\pm}^{\nu_{\pm}}} (1 + o(1)) \text{ for } \nu_{\pm} > 0 \text{ near } x' = \Lambda', \end{aligned} \quad (12)$$

where $a' = \frac{1}{2}\overline{AB} = \varepsilon'/2$ is the radius of the gap, and the constants ℓ_{\pm} have dimension of length. For $\nu_{\pm} = 1$ the parameters ℓ_{\pm} are the radii of curvature R_c^{\pm} at $x' = \Lambda'$. To simplify the conformal mapping, we first rotate the domain by $\pi/2$ clockwise to assume the shape in Figure 2(left). The rotated axes are renamed (x', y') as well.

The NET of Brownian motion with diffusion coefficient D from a point $\mathbf{x}' = (x', y')$ inside the domain Ω' with reflection at the boundary $\partial\Omega'$, except for an absorbing boundary $\partial\Omega'_a$ at the bottom of the neck, is the solution of the boundary value problem

$$\begin{aligned} D\Delta\bar{u}(\mathbf{x}') &= -1 \text{ for } \mathbf{x}' \in \Omega' \\ \frac{\partial\bar{u}(\mathbf{x}')}{\partial n} &= 0 \text{ for } \mathbf{x}' \in \partial\Omega' - \partial\Omega'_a \\ \bar{u}(\mathbf{x}') &= 0 \text{ for } \mathbf{x}' \in \partial\Omega'_a. \end{aligned} \quad (13)$$

We convert to dimensionless variables by setting $\mathbf{x}' = \ell_+\mathbf{x}$, $\Lambda' = \ell_+\Lambda$, the domain Ω' is mapped into Ω and we have (see (14) below)

$$|\Omega'| = \ell_+^2|\Omega|, \quad |\partial\Omega'| = \ell_+|\partial\Omega|, \quad |\partial\Omega'_a| = \varepsilon' = \ell_+|\partial\Omega_a| = \ell_+\varepsilon. \quad (14)$$

Setting $\bar{u}(\mathbf{x}') = u(\mathbf{x})$, we write (13) as

$$\begin{aligned} \frac{D}{\ell_+^2}\Delta u(\mathbf{x}) &= -1 \text{ for } \mathbf{x} \in \Omega \\ \frac{\partial u(\mathbf{x})}{\partial n} &= 0 \text{ for } \mathbf{x} \in \partial\Omega - \partial\Omega_a \\ u(\mathbf{x}) &= 0 \text{ for } \mathbf{x} \in \partial\Omega_a. \end{aligned} \quad (15)$$

2.1 Asymptotic analysis

First, we consider the case $\nu_{\pm} = 1$, $\ell_+ = R_c$, and $\ell_- = r_c$, radius 1, and A has dimensionless radius r_c/R_c . This case can represent a partial block described in Figure 3. With the scaling

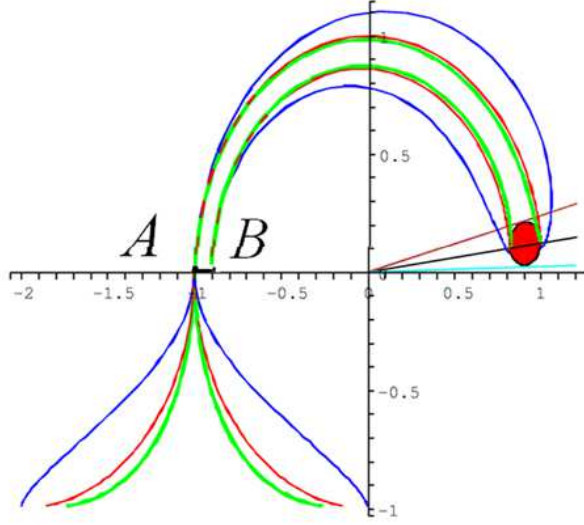


Figure 5: The image in $\Omega_w = w(\Omega)$ of the necks AB in Figure 2 under the conformal mapping (16). The funnel in Figure 2 (shown inverted in the third quadrant) is mapped onto the ring enclosed between the like-colored arcs and the large disk is mapped onto small red disk. The short black segment AB (of length ε) is mapped onto the thick black segment \mathbf{AB} (of length $2\sqrt{\varepsilon} + O(\varepsilon)$).

(14) the bounding circle B has dimensionless We construct an asymptotic solution for small gap ε by first mapping the domain Ω in Figure 2(left) conformally into its image under the Möbius transformation of the two bounding circles (thin line) into concentric circles. To this end we move the origin of the complex plane to the center of the right lower circle and set

$$w = w(z) = \frac{z - \alpha}{1 - \alpha z}, \quad (16)$$

where

$$\begin{aligned} \alpha &= -\frac{2\varepsilon R_c + 2R_c + \varepsilon^2 R_c + 2r_c \varepsilon + 2r_c}{2(\varepsilon R_c + r_c + R_c)} \\ &\quad \pm \frac{\sqrt{\varepsilon(8R_c r_c + 4\varepsilon R_c^2 + 12\varepsilon R_c r_c + 4\varepsilon^2 R_c^2 + 8r_c^2 + 4\varepsilon^2 R_c r_c + \varepsilon^3 R_c^2 + 4\varepsilon r_c^2)}}{2(\varepsilon R_c + r_c + R_c)} \\ &= -1 \pm \sqrt{\frac{2r_c \varepsilon}{R_c + r_c}} + O(\varepsilon), \end{aligned} \quad (17)$$

which maps the right lower circle into itself and Ω is mapped onto the domain $\Omega_w = w(\Omega)$ in Figure 5. The straits in Figure 2(left) are mapped onto the ring enclosed between the like-colored arcs and the large disk is mapped onto the small red disk. The radius of the small red disk and the elevation of its center above the real axis are $O(\sqrt{\varepsilon})$. The short black segment of length ε in Figure 2 is mapped onto a segment of length $2\sqrt{\varepsilon} + O(\varepsilon)$.

Setting $u(z) = v(w)$ and $\tilde{\varepsilon} = 2r_c\varepsilon/(R_c + r_c)$, the system (15) is converted to

$$\begin{aligned}\Delta_w v(w) &= -\frac{\ell_+^2}{D|w'(z)|^2} = -\frac{(4\tilde{\varepsilon} + O(\tilde{\varepsilon}^{3/2}))\ell_+^2}{D|w(1 - \sqrt{\tilde{\varepsilon}}) - 1 + O(\tilde{\varepsilon})|^4} \text{ for } w \in \Omega_w \\ \frac{\partial v(w)}{\partial n} &= 0 \text{ for } w \in \partial\Omega_w - \partial\Omega_{w,a} \\ v(w) &= 0 \text{ for } w \in \partial\Omega_{w,a}.\end{aligned}\tag{18}$$

The MFPT is bounded above and below by that from the inverse image of a circular ring cut by lines through the origin, tangent to the red disk at polar angles $\theta = c_1\sqrt{\tilde{\varepsilon}}$ (brown) and $\theta = c_2\sqrt{\tilde{\varepsilon}}$ (cyan) for some positive constants c_1, c_2 , independent of $\tilde{\varepsilon}$. Therefore the MFPT from Ω equals that from the inverse image of a ring cut by an intermediate angle $\theta = c\sqrt{\tilde{\varepsilon}}$ (black).

The asymptotic analysis of (18) begins with the observation that the solution of the boundary value problem (18) is to leading order independent of the radial variable in polar coordinates $w = re^{i\theta}$. Fixing $r = 1$, we impose the reflecting boundary condition at $\theta = c\sqrt{\tilde{\varepsilon}}$, where $c = O(1)$ is a constant independent of $\tilde{\varepsilon}$ to leading order, and the absorbing condition at $\theta = \pi$. The outer solution, obtained by a regular expansion of $v(e^{i\theta})$, is given by

$$v_0(e^{i\theta}) = A(\theta - \pi),\tag{19}$$

where A is yet an undetermined constant. It follows that

$$\left. \frac{\partial v_0(e^{i\theta})}{\partial \theta} \right|_{\theta=\pi} = -A.\tag{20}$$

To determine A , we integrate (18) over the domain to obtain at the leading order

$$2\sqrt{\tilde{\varepsilon}} \left. \frac{\partial v_0(e^{i\theta})}{\partial \theta} \right|_{\theta=\pi} = -2\sqrt{\tilde{\varepsilon}}A \sim -\frac{|\Omega'|}{D},\tag{21}$$

hence

$$A \sim \frac{|\Omega'|}{2D\sqrt{\tilde{\varepsilon}}}.\tag{22}$$

Now (19) gives for $\theta = c\sqrt{\tilde{\varepsilon}}$ the leading order approximation

$$\bar{\tau} \sim A\pi = \frac{\pi|\Omega'|}{D\sqrt{\tilde{\varepsilon}}}.\tag{23}$$

The following more explicit analysis was briefly summarized in [15] for the symmetric case $\nu_{\pm} = 1, R_c = r_c$ and is explicitly given here for completeness. The leading order approximation is obtained by an explicit integration of (18) with respect to θ ,

$$v(e^{i\theta}) = \frac{4\ell_+^2\tilde{\varepsilon}}{D} \int_{\theta}^{\pi} d\varphi \int_{c\sqrt{\tilde{\varepsilon}}}^{\varphi} \frac{d\eta}{|e^{i\eta} - 1 - e^{i\eta}\sqrt{\tilde{\varepsilon}}|^4},\tag{24}$$

so that

$$\begin{aligned}
v\left(e^{ic\sqrt{\tilde{\varepsilon}}}\right) &= \frac{4\ell_+^2\tilde{\varepsilon}}{D} \int_{c\sqrt{\tilde{\varepsilon}}}^{\pi} d\varphi \int_{\varphi}^{\pi} \frac{d\eta}{|e^{i\eta} - 1 - e^{i\eta}\sqrt{\tilde{\varepsilon}}|^4} \\
&= \frac{4\ell_+^2\tilde{\varepsilon}}{D} \int_{c\sqrt{\tilde{\varepsilon}}}^{\pi} \frac{(\pi - \eta) d\eta}{|e^{i\eta} - 1 - e^{i\eta}\sqrt{\tilde{\varepsilon}}|^4}.
\end{aligned} \tag{25}$$

First, we evaluate asymptotically the integral

$$\frac{\ell_+^2\tilde{\varepsilon}}{D} \int_{c\sqrt{\tilde{\varepsilon}}}^{\pi} \frac{\eta d\eta}{|e^{i\eta} - 1 - e^{i\eta}\sqrt{\tilde{\varepsilon}}|^4} \tag{26}$$

by setting $\eta = \sqrt{\tilde{\varepsilon}}\zeta$ and noting that

$$\left| \frac{e^{i\zeta\sqrt{\tilde{\varepsilon}}} - 1}{i\zeta\sqrt{\tilde{\varepsilon}}} - 1 \right| = \left| \frac{-2\sin^2\frac{\zeta\sqrt{\tilde{\varepsilon}}}{2}}{i\zeta\sqrt{\tilde{\varepsilon}}} + \frac{\sin\zeta\sqrt{\tilde{\varepsilon}}}{\zeta\tilde{\varepsilon}} - 1 \right| = O(\zeta\sqrt{\tilde{\varepsilon}}) \text{ for all } \eta, \tilde{\varepsilon} > 0. \tag{27}$$

It follows that

$$\frac{4\ell_+^2\tilde{\varepsilon}}{D} \int_{c\sqrt{\tilde{\varepsilon}}}^{\pi} \frac{\eta d\eta}{|e^{i\eta} - 1 - e^{i\eta}\sqrt{\tilde{\varepsilon}}|^4} = \frac{4\ell_+^2}{D} \int_c^{\pi/\sqrt{\tilde{\varepsilon}}} \frac{\zeta d\zeta}{|1 + \zeta^2 + O(\tilde{\varepsilon}\zeta^2)|^2} = \frac{4}{D(c+1)} \left(1 + O(\sqrt{\tilde{\varepsilon}})\right). \tag{28}$$

Similarly, we obtain that

$$\frac{4\tilde{\varepsilon}}{D} \int_{c\sqrt{\tilde{\varepsilon}}}^{\pi} \frac{d\eta}{|e^{i\eta} - 1 - e^{i\eta}\sqrt{\tilde{\varepsilon}}|^4} = \frac{4}{D\sqrt{\tilde{\varepsilon}}} \int_c^{\pi/\sqrt{\tilde{\varepsilon}}} \frac{d\zeta}{|1 + \zeta^2 + O(\tilde{\varepsilon}\zeta^2)|^2} = \frac{C}{D\sqrt{\tilde{\varepsilon}}} \left(1 + O(\sqrt{\tilde{\varepsilon}})\right), \tag{29}$$

where $C = O(1)$ is a constant, so that

$$v\left(e^{ic\sqrt{\tilde{\varepsilon}}}\right) = \frac{4\ell_+^2\pi C}{D\sqrt{\tilde{\varepsilon}}} \left(1 + O(\sqrt{\tilde{\varepsilon}})\right). \tag{30}$$

To determine the value of the constant C , we note that (24) implies that

$$\left. \frac{\partial v(e^{i\theta})}{\partial n} \right|_{\partial\Omega_{w,a}} = \left. \frac{\partial v}{\partial \theta} \right|_{\theta=\pi} = -\frac{4\ell_+^2\tilde{\varepsilon}}{D} \int_{c\sqrt{\tilde{\varepsilon}}}^{\pi} \frac{d\eta}{|e^{i\eta} - 1 - e^{i\eta}\sqrt{\tilde{\varepsilon}}|^4} = -\frac{4\ell_+^2 C}{D\sqrt{\tilde{\varepsilon}}} \left(1 + O(\sqrt{\tilde{\varepsilon}})\right) \tag{31}$$

and the integration of (18) over Ω_w gives

$$2\sqrt{\tilde{\varepsilon}} \left. \frac{\partial v(e^{i\theta})}{\partial n} \right|_{\partial\Omega_{w,a}} = -\frac{\ell_+^2 |\Omega|}{D}. \quad (32)$$

Now, (31) and (32) imply that $4C = |\Omega|/2$, so that the MFPT to the straits, $\bar{\tau}$, is

$$\bar{\tau} = \frac{\ell_+^2 \pi |\Omega|}{2D\sqrt{\tilde{\varepsilon}}} (1 + o(1)) = \frac{\pi |\Omega'|}{2D\sqrt{\tilde{\varepsilon}}} (1 + o(1)) \quad \text{for } \tilde{\varepsilon} \ll |\partial\Omega|, \ell_+, \quad (33)$$

which is (23). In dimensional units (33) becomes

$$\bar{\tau} = \sqrt{\frac{R_c(R_c + r_c)}{2r_c \varepsilon'}} \frac{\pi |\Omega'|}{2D} (1 + o(1)) \quad \text{for } \varepsilon' \ll |\partial\Omega'|, R_c, r_c. \quad (34)$$

In the symmetric case $R_c = r_c$ (34) reduces to the result of [15]

$$\bar{\tau} = \frac{\pi |\Omega'|}{2D\sqrt{\varepsilon'/R_c}} (1 + o(1)) \quad \text{for } \varepsilon' \ll |\partial\Omega'|, R_c. \quad (35)$$

Next, we consider for simplicity the symmetric case $\nu_+ = \nu_- > 1$, so $R_c = r_c = \infty$. After scaling the boundary value problem (13) with (14), we can choose the bounding circles at A and B to have radius 1 and repeat the above analysis in the domain Ω_w enclosed by the green curves, shown in Figure (5). The result (35) becomes

$$\bar{\tau} = \frac{\pi |\Omega'|}{2D\sqrt{\varepsilon'/\ell_+}} (1 + o(1)) \quad \text{for } \varepsilon' \ll |\partial\Omega'|, \ell_+. \quad (36)$$

2.2 Exit from several bottlenecks

In case of exit through any one of N well-separated necks with dimensionless curvature parameters l_j and widths $\tilde{\varepsilon}_j$, we construct the outer solution (19) at any one of the N absorbing windows so that (20) holds at each window. The integration of (18) over Ω gives the following analog of (21),

$$\sum_{j=1}^N 2\sqrt{\tilde{\varepsilon}_j} \left. \frac{\partial v_0(e^{i\theta})}{\partial \theta} \right|_{\theta=\pi} = -2 \sum_{j=1}^N \sqrt{\tilde{\varepsilon}_j} A \sim -\frac{|\Omega'|}{D}, \quad (37)$$

hence

$$A \sim \frac{|\Omega'|}{2D \sum_{j=1}^N \sqrt{\tilde{\varepsilon}_j}}. \quad (38)$$

Equation (33) is then generalized to

$$\bar{\tau} = \frac{\pi |\Omega'|}{2D \sum_{j=1}^N \sqrt{\varepsilon'_j/\ell_j}} (1 + o(1)) \quad \text{for } \varepsilon'_j/\ell_j \ll |\partial\Omega|. \quad (39)$$

Equations (34)-(36) are generalized in a similar manner.

To calculate the exit probability through any one of the N necks, we apply the transformation (16) separately for each bottleneck at the absorbing images $\partial\Omega_{w,a_1}, \dots, \partial\Omega_{w,a_N}$ to obtain images Ω_{w_j} for $j = 1, 2, \dots, N$. Then the probability of exiting through $\partial\Omega_{w,a_i}$ is the solution of the mixed boundary value problem

$$\begin{aligned} \Delta_w v(w) &= 0 \text{ for } w \in \Omega_{w_i} \\ \frac{\partial v(w)}{\partial n} &= 0 \text{ for } w \in \partial\Omega_{w_i} - \bigcup_{i=1}^N \partial\Omega_{w,a_i} \\ v(w) &= 1 \text{ for } w \in \partial\Omega_{w,a_i} \\ v(w) &= 0 \text{ for } w \in \partial\Omega_{w,a_j}, j \neq i. \end{aligned} \tag{40}$$

The outer solution, which is the exit probability through window $\partial\Omega_{w,i}$, is an unknown constant p_i . We construct boundary layers at each absorbing boundary $\partial\Omega_{w,a_j}$ for $j \neq i$ by solving the boundary value problem in Ω_{w_j} , which is of the type shown in Figure 5 with a neck of width ε_j . In each case the boundary layer is a linear function

$$v_j(\theta) = \delta_{i,j} - A_j(\theta - \pi) \text{ for all } j, \tag{41}$$

such that

$$v_j(0) \sim \delta_{i,j} + A_j\pi = p_i \text{ for all } j. \tag{42}$$

To determine the value of the constant p_i , we note that

$$\left. \frac{\partial v(e^{i\theta})}{\partial n} \right|_{\partial\Omega_{w,a}} = \left. \frac{\partial v_j(\theta)}{\partial \theta} \right|_{\theta=\pi} = -A_j, \tag{43}$$

so the integration of (40) over Ω_{w_i} gives

$$\sum_{j=1}^N A_j |\partial\Omega_{w,a_j}| = \sum_{j=1}^N 2A_j \sqrt{\tilde{\varepsilon}_j} = 0. \tag{44}$$

The $N + 1$ equations (42) and (44) for the unknowns p_i, A_1, \dots, A_N give the exit probability from an interior point in the planar case as

$$p_i = \frac{\sqrt{\varepsilon'_i/\ell_i}}{\sum_{j=1}^N \sqrt{\varepsilon'_j/\ell_j}}. \tag{45}$$

3 The NET in a solid funnel-shaped domain

We consider now the NET problem in the solid of revolution obtained by rotating the symmetric domain Ω' in Figure 2(left) about its axis of symmetry. The absorbing end of the

neck becomes a circular disk of radius $a' = \varepsilon'/2$. Due to cylindrical symmetry of the mixed boundary value problem (15) the MFPT in cylindrical coordinates centered on the axis of symmetry is independent of the angle. It follows that with the scaling (14) the boundary value problem (15) in the scaled spatial domain Ω can be written in cylindrical coordinates as

$$\Delta u = \frac{\partial^2 u}{\partial r^2} + \frac{1}{r} \frac{\partial u}{\partial r} + \frac{\partial^2 u}{\partial z^2} = -\frac{\ell_+^2}{D}. \quad (46)$$

Equation (46) can be considered as a two-dimensional problem in the planar cross section by a plane through the axis of symmetry of Ω in the (r, z) plane. Here r is the distance to the axis of symmetry of Ω , the z axis is perpendicular to that axis and the origin is inside the cross section of Ω , at the intersection of the axis with the tangent to the osculating circle to the cross section at the gap. Setting $u_1 = ur^{1/2}$, the MFPT equation (46) takes the form

$$\frac{\partial^2 u_1(r, z)}{\partial r^2} + \frac{\partial^2 u_1(r, z)}{\partial z^2} = -\frac{\ell_+^2}{D} \left(r^{1/2} + \frac{u_1(r, z)}{4r^2} \right) \quad (47)$$

in the cross section, with mixed Neumann-Dirichlet boundary conditions, as in the planar case. We assume that in dimensionless variables $\overline{AB} = \varepsilon \ll 1 < |\Omega|^{1/3}$, so the funnel is a narrow passage. The transformation to the rotated and translated coordinates is given by $\tilde{r} = r - 1 - \varepsilon/2$, $\tilde{z} = -z + 1$. Setting $u_1(r, z) = \tilde{u}(\tilde{r}, \tilde{z})$, equation (47) becomes

$$\frac{\partial^2 \tilde{u}(\tilde{r}, \tilde{z})}{\partial \tilde{r}^2} + \frac{\partial^2 \tilde{u}(\tilde{r}, \tilde{z})}{\partial \tilde{z}^2} = -\frac{\ell_+^2}{D} \left(\left(\tilde{r} + 1 + \frac{\varepsilon}{2} \right)^{1/2} - \frac{\tilde{u}(\tilde{r}, \tilde{z})}{4 \left(\tilde{r} + 1 + \frac{\varepsilon}{2} \right)^2} \right). \quad (48)$$

3.1 Asymptotic solution

We construct an asymptotic solution for small gap ε by first mapping the cross section in the (r, z) -plane conformally into its image under the Möbius transformation (16),

$$w(\zeta) = \rho e^{i\eta} = \frac{\zeta - \alpha}{1 - \alpha\zeta}, \quad (49)$$

where α is given in (17) for the symmetric case $R_c = r_c = 1$. Setting $\tilde{u}(\zeta) = v(w)$, equation (48) becomes

$$\Delta_w v(w) = \frac{\ell_+^2}{D|w'(\zeta)|^2} \left(-\left| \operatorname{Re} \frac{w + \alpha}{1 + \alpha w} + 1 + \frac{\varepsilon}{2} \right|^{1/2} - \frac{v}{4 \left| \operatorname{Re} \frac{w + \alpha}{1 + \alpha w} + 1 + \frac{\varepsilon}{2} \right|^2} \right). \quad (50)$$

Because the normalized head of Figure 2(left) is mapped into the narrow hot dog-shaped region in Figure 5 of width $\sqrt{\varepsilon}$ at $\rho = 1$, we approximate

$$w = e^{i\eta} + O(\sqrt{\varepsilon}), \quad \left| \frac{w + \alpha}{1 + \alpha w} \right| = 1 + O(\sqrt{\varepsilon}). \quad (51)$$

We also have

$$w'(\zeta) = \frac{(1 + \alpha w)^2}{\alpha^2 - 1} \quad (52)$$

$$|w'(\zeta)|^2 = \left| \frac{(1 + w\alpha)^2}{1 - \alpha^2} \right|^2 = \frac{|1 - w + \sqrt{\varepsilon} w|^4}{4\varepsilon} (1 + O(\sqrt{\varepsilon})), \quad (53)$$

so that (47) reduces to

$$\Delta_w v = -\frac{\ell_+^2}{D} \frac{4\varepsilon(1 + O(\sqrt{\varepsilon}))}{|1 - w + \sqrt{\varepsilon} w|^4} \left(\sqrt{2} + \frac{1}{16}v \right), \quad (54)$$

or equivalently,

$$v'' + \frac{\varepsilon}{4|e^{i\eta} - 1 - e^{i\eta}\sqrt{\varepsilon}|^4} v = \frac{\ell_+^2}{D} \frac{4\sqrt{2}\varepsilon}{|e^{i\eta} - 1 - e^{i\eta}\sqrt{\varepsilon}|^4} (1 + O(\sqrt{\varepsilon})). \quad (55)$$

Setting $v = \ell_+^2 (y - 16\sqrt{2})/D$, we obtain the leading order equation

$$y''(\eta) + \frac{\varepsilon}{4|e^{i\eta} - 1 - e^{i\eta}\sqrt{\varepsilon}|^4} y(\eta) = 0. \quad (56)$$

The boundary conditions are

$$y'(c\sqrt{\varepsilon}) = 0, \quad y(\pi) = 16\sqrt{2}. \quad (57)$$

The outer solution is the linear function

$$y_{\text{outer}}(\eta) = M\eta + N, \quad (58)$$

where M and N are yet undetermined constants. The absorbing boundary condition in (57) gives

$$y_{\text{outer}}(\pi) = M\pi + N = 16\sqrt{2}. \quad (59)$$

A boundary layer correction is needed to satisfy the boundary conditions at the reflecting boundary at $\eta = c\sqrt{\varepsilon}$. To resolve the boundary layer at $\eta = c\sqrt{\varepsilon}$, we set $\eta = \sqrt{\varepsilon}\xi$ and expand

$$\frac{\varepsilon^2}{|e^{i\eta} - 1 - e^{i\eta}\sqrt{\varepsilon}|^4} = \frac{1}{(1 + \xi^2)^2} + O(\sqrt{\varepsilon}).$$

Writing $y_{\text{bl}}(\eta) = Y(\xi)$, we obtain to leading order the boundary layer equation

$$Y''(\xi) + \frac{1}{4(1 + \xi^2)^2} Y(\xi) = 0, \quad (60)$$

which has two linearly independent solutions, $Y_1(\xi)$ and $Y_2(\xi)$ that are linear functions for sufficiently large ξ . Initial conditions for $Y_1(\xi)$ and $Y_2(\xi)$ can be chosen so that $Y_2(\xi) \rightarrow \text{const}$ as $\xi \rightarrow \infty$ (e.g., $Y_2(0) = -4.7$, $Y_2'(0) = -1$, see Figure 6). Setting

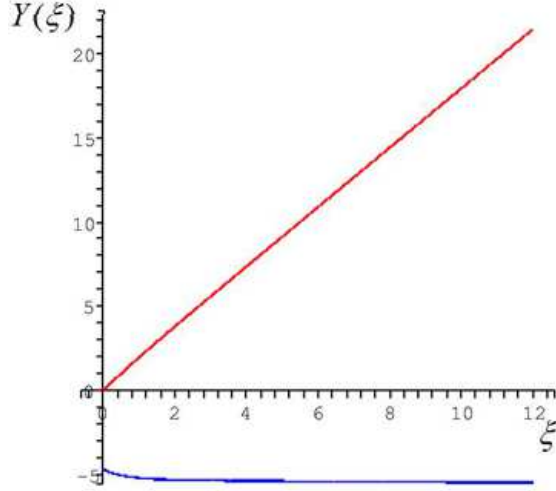


Figure 6: Two linearly independent solutions of (60). The linearly growing solution $Y_1(\xi)$ (red) satisfies the initial conditions $Y_1(0) = 0$, $Y_1'(0) = 2$. The asymptotically constant solution $Y_2(\xi)$ (blue) satisfies the initial conditions $Y_2(0) = -4.7$, $Y_2'(0) = -1$. The asymptotic value is $Y_2(\infty) \approx -5$.

$$y_{\text{bl}}(\eta) = AY_1\left(\frac{\eta}{\sqrt{\varepsilon}}\right) + BY_2\left(\frac{\eta}{\sqrt{\varepsilon}}\right), \quad (61)$$

where A and B are constants to be determined, we seek a uniform approximation to $y(\eta)$ in the form $y_{\text{unif}}(\eta) = y_{\text{outer}}(\eta) + y_{\text{bl}}(\eta)$. The matching condition is that $AY_1(\eta/\sqrt{\varepsilon}) + BY_2(\eta/\sqrt{\varepsilon})$ remains bounded as $\xi \rightarrow \infty$, which implies $A = 0$. It follows that at the absorbing boundary $\eta = \pi$ we have

$$\begin{aligned} y_{\text{unif}}(\pi) &= M\pi + \beta - 5B = 16\sqrt{2} \\ y'_{\text{unif}}(\pi) &= M. \end{aligned} \quad (62)$$

At the reflecting boundary we have to leading order

$$y'_{\text{unif}}(c\sqrt{\varepsilon}) = y'_{\text{outer}}(c\sqrt{\varepsilon}) + y'_{\text{bl}}(c\sqrt{\varepsilon}) = M + B\frac{Y_2'(c)}{\sqrt{\varepsilon}} = 0, \quad (63)$$

which gives

$$B = -\frac{M\sqrt{\varepsilon}}{Y_2'(c)}, \quad N = 16\sqrt{2} - \frac{5M\sqrt{\varepsilon}}{Y_2'(c)} - M\pi. \quad (64)$$

The uniform approximation to $v(w)$ is given by

$$v_{\text{unif}}(\rho e^{i\eta}) = M\left(\eta - \pi - \frac{5\sqrt{\varepsilon}}{Y_2'(c)}\right), \quad (65)$$

so that using (52), we obtain from (65)

$$\left. \frac{\partial u}{\partial n} \right|_{\zeta \in \partial\Omega_a} = \left. \frac{\partial v(\rho e^{i\eta})}{\partial \eta} \right|_{\eta=\pi} w'(\zeta) \Big|_{\zeta=-1} = \frac{2M}{\sqrt{\varepsilon}} (1 + O(\sqrt{\varepsilon})). \quad (66)$$

To determine the value of M , we integrate (15) over Ω , use (66), and the fact that

$$\int_{\partial\Omega_a} dS = \frac{\pi\varepsilon^2}{4}, \quad (67)$$

to obtain $M = -2\ell_+^2 |\Omega| / D\pi\varepsilon^{3/2}$. Now (65) gives the MFPT at any point \mathbf{x} in the head as

$$\bar{\tau} = u(\mathbf{x}) \sim v(\rho e^{c\sqrt{\varepsilon}}) \sim 2\varepsilon^{-3/2} \frac{\ell_+^2 |\Omega|}{D} = 2\varepsilon^{-3/2} \frac{|\Omega'|}{\ell_+ D} \text{ for } \varepsilon \ll 1. \quad (68)$$

The dimensional radius of the absorbing end of the funnel is $a' = \ell_+ \varepsilon / 2$ (see (14)), so (68) can be written in physical units as

$$\bar{\tau} = \frac{1}{\sqrt{2}} \left(\frac{\ell_+}{a'} \right)^{3/2} \frac{V}{\ell_+ D} (1 + o(1)) \text{ for } a' \ll \ell_+, \quad (69)$$

where $V = |\Omega'|$ is the volume of the domain.

3.2 Exit from several bottlenecks

The generalization of (69) to exit through N well-separated necks is found by noting that (67) becomes

$$\int_{\partial\Omega_a} dS = \sum_{j=1}^N \frac{\pi\varepsilon_j^2}{4}, \quad (70)$$

and the integration of (13) over Ω' gives the compatibility condition (dimensional)

$$\int_{\partial\Omega'} \frac{\partial u(\mathbf{x}')}{\partial n'} dS' = M \sum_{j=1}^N \frac{\ell_j \pi \varepsilon_j^2}{4\sqrt{\varepsilon_j}} = -\frac{|\Omega'|}{D} \quad (71)$$

which determines

$$M = -\frac{4|\Omega'|}{D \sum_{j=1}^N \ell_j \pi \varepsilon_j^{3/2}}. \quad (72)$$

Hence, using the dimensional $a'_j = \ell_j \varepsilon_j / 2$, we obtain

$$\bar{\tau} = -M\pi = \frac{1}{\sqrt{2}} \frac{|\Omega'|}{D \sum_{j=1}^N \ell_j \left(\frac{a'_j}{\ell_j} \right)^{3/2}}. \quad (73)$$

To calculate the exit probability from one of N necks, we note that the boundary layer function is to leading order linear, as in Section 2.2. Therefore in the three-dimensional case the exit probability is given by

$$p_i = \frac{\varepsilon_i^{3/2} \ell_i}{\sum_{j=1}^N \varepsilon_j^{3/2} \ell_j} = \frac{a_i'^{3/2} \ell_i^{-1/2}}{\sum_{j=1}^N a_j'^{3/2} \ell_j^{-1/2}}. \quad (74)$$

4 Diffusion and NET on a surface of revolution

We consider now Brownian motion on a surface of revolution generated by rotating the curve in Figure 2(left) about its axis of symmetry and assume $\nu_+ = \nu_- = \nu$ and $\ell_+ = \ell_- = \ell$. The projection of the Brownian motion from the surface to the z -axis gives rise to a drift. The backward Kolmogorov operator [22] of the projected motion, scaled with (14), is given by

$$\mathcal{L}^* u(z) = \frac{D}{\ell^2} \left\{ \frac{1}{1+r'^2(z)} u''(z) + \left[\frac{r'(z)}{r(z)(1+r'(z)^2)} - \frac{r'(z)r''(z)}{(1+r'(z)^2)^2} \right] u'(z) \right\}. \quad (75)$$

The operator \mathcal{L}^* corresponds to the Itô equation

$$dz = a(z) dt + b(z) dw, \quad (76)$$

where the drift $a(z)$ and noise intensity $b(z)$ are given by

$$a(z) = \frac{D}{\ell^2} \left\{ \frac{r'(z)}{r(z)(1+r'(z)^2)} - \frac{r'(z)r''(z)}{(1+r'(z)^2)^2} \right\}, \quad b(z) = \sqrt{\frac{2D}{\ell^2(1+r'^2(z))}} \quad (77)$$

and $w(t)$ is standard Brownian motion on the line. The potential of the drift is $A(z) = -\int_{\Lambda}^z a(t) dt$.

To calculate the MFPT from $z = 0$ to the end of the funnel at $z = \Lambda$, we note that due to rotational symmetry the solution of the Andronov-Pontryagin-Vitt boundary value problem [22] for the MFPT $u(z, \theta)$ on the surface is independent of θ . Therefore the problem reduces to

$$\frac{1}{r(z)\sqrt{1+r'^2(z)}} \frac{\partial}{\partial z} \left[\frac{r(z)}{\sqrt{1+r'^2(z)}} \frac{\partial u(z)}{\partial z} \right] = -\frac{\ell^2}{D} \quad (78)$$

$$u'(0) = u(\Lambda) = 0.$$

The MFPT is given by

$$u(0) = \frac{\ell^2}{2\pi D} \int_{\Lambda}^0 \frac{\sqrt{1+r'^2(t)}}{r(t)} S(t) dt. \quad (79)$$

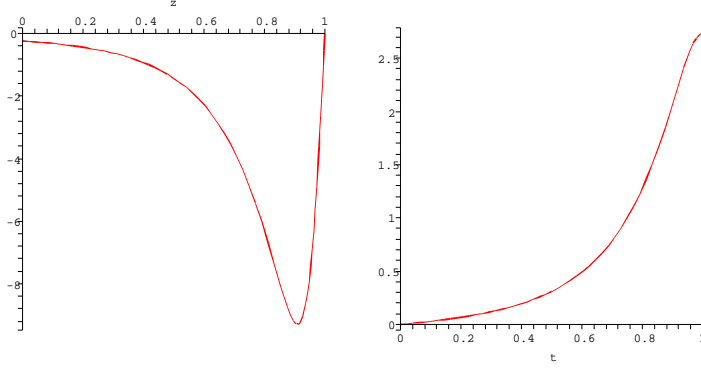


Figure 7: The drift $a(z)$ in (77) (left panel) and its potential $A(z)$ (right panel) near the cusp. The projection of the Brownian motion on the axis of symmetry has an effective high barrier in the neck.

where $S(t)$ is the (scaled) area of the surface of revolution from $z = t$ to $z = 0$, given by

$$S(t) = 2\pi \int_t^0 r(s) \sqrt{1 + r'^2(s)} ds. \quad (80)$$

The main contribution to (79) comes from $\Lambda < t < \Lambda + \delta$ for a sufficiently small δ , such that $\delta \gg a$ (note that the singularity of $1/r(z)$ near $z = 0$ is integrable). Thus (79) and (80) give for $\nu > 0$

$$\bar{\tau} = u(0) \sim \frac{\ell^2 S(\Lambda)}{2\pi D} \int_{\Lambda}^{\Lambda+\delta} \frac{\sqrt{1 + r'^2(t)}}{r(t)} dt \sim \frac{\mathcal{S}(\Lambda)}{2D} \frac{\left(\frac{\ell}{(1+\nu)a}\right)^{\nu/1+\nu} \nu^{1/1+\nu}}{\sin \frac{\nu\pi}{1+\nu}}, \quad (81)$$

where $\mathcal{S} = \mathcal{S}(\Lambda)$ is the entire unscaled area of the surface. In particular, for $\nu = 1$ we get the MFPT

$$\bar{\tau} \sim \frac{\mathcal{S}}{4D\sqrt{a/2\ell}}. \quad (82)$$

The case $\nu = 0$ corresponds to an absorbing circular cap of a small radius a on a closed surface. For a sphere the solution of (78) gives the known result

$$\bar{\tau}_{\mathbf{x} \rightarrow \partial\Omega_i} = \frac{2R^2}{D} \log \frac{\sin \frac{\theta}{2}}{\sin \frac{\delta}{2}}, \quad (83)$$

where θ is the angle between \mathbf{x} and the south-north axis of the sphere and $a = R \sin \delta/2$ (see [8]–[11]). If a right circular cylinder of a small radius a and length $L' = \ell L$ is attached

to the surface at $z = \Lambda$, then the integration in (81) extends now to $\Lambda - L$, giving

$$\begin{aligned} u(0) &\sim \frac{\ell^2 \mathcal{S}(\Lambda)}{2\pi D} \int_{\Lambda}^0 \frac{\sqrt{1+r'^2(t)}}{r(t)} dt + \frac{\ell^2}{2\pi D a} \int_{\Lambda-L}^{\Lambda} [S(\Lambda) + 2\pi a(t - \Lambda)] dt \\ &= \frac{\mathcal{S}(\Lambda)}{2\pi D} \int_{\Lambda}^0 \frac{\sqrt{1+r'^2(t)}}{r(t)} dt + \frac{\mathcal{S}(\Lambda)L'}{2\pi D a} + \frac{L'^2}{2D}, \end{aligned} \quad (84)$$

where the integral is given by (81), (82), or (83) for the various values of ν . Note that while \bar{r} on the surface depends on the fractional power $-\nu/(1+\nu)$ of the neck's radius a , the power of a in the three-dimensional case is $-3/2$, as indicated in (69).

The case $\nu = 0$ is not the limit of (81), because the line (5) blows up. This case corresponds to a conical funnel with an absorbing circle of small radius a and length H (see Figure 4). We assume that the radius of the other base of the cone, b , is smaller than a , but that $b \ll \mathcal{S}^{1/2}$. The generator of the cone is the line segment

$$r(x) = a + C(x - L) \text{ for } \Lambda - L < x < \Lambda, \quad (85)$$

where C is the (positive) slope. In this case (84) is replaced by

$$\begin{aligned} u(0) &= \frac{\mathcal{S}(\Lambda)}{2\pi D} \int_{\Lambda}^0 \frac{\sqrt{1+r'^2(t)}}{r(t)} dt + \frac{\mathcal{S}(\Lambda)\sqrt{1+C^2}}{2\pi DC} \log \left(1 + \frac{CL'}{a} \right) \\ &\quad + \frac{(1+C^2)}{2DC^2} \left[(a + CL') \log \left(1 + \frac{CL'}{a} \right) + \frac{1}{2}[(a + CL')^2 - a^2] \right], \end{aligned}$$

which reduces to (84) in the limit $CL' \ll a$ and for $a \ll CL'$ can be simplified to leading order to

$$\begin{aligned} u(0) &= \frac{\mathcal{S}(\Lambda)}{2\pi D} \int_{\Lambda}^0 \frac{\sqrt{1+r'^2(t)}}{r(t)} dt + \frac{\mathcal{S}(\Lambda)\sqrt{1+C^2}}{2\pi DC} \log \frac{CL'}{a} \\ &\quad + \frac{(1+C^2)L'^2}{2D} \log \frac{CL'}{a} + O(1). \end{aligned} \quad (86)$$

Note that the last term in (86) blows up as $a \rightarrow 0$ while that in (84) does not. This is due to the degeneration of the NET problem in the cylinder, as noted in [6].

5 The principal eigenvalue in domains with bottlenecks

The narrow escape time is related to the leading eigenvalues of the Neumann or mixed Neumann-Dirichlet problem for the Laplace equation in domains that consists of compartments and narrow necks. In domains that consists of compartments interconnected by narrow

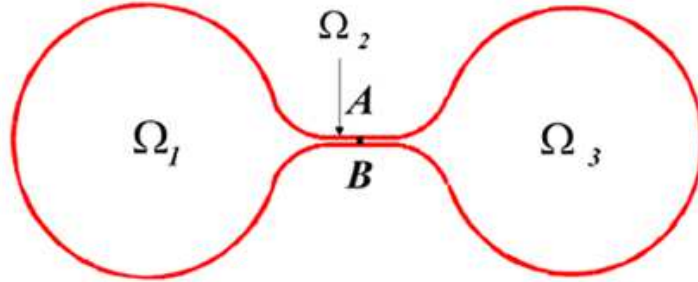


Figure 8: A dumbbell-shaped domain consists of two large compartments Ω_1 and Ω_3 connected by a narrow neck Ω_2 . The bottleneck is the interval \mathbf{AB} .

necks the MFPT from one compartment to the other, as defined in [18], is to leading order (in the limit of shrinking neck) independent of the initial point of the escaping trajectory and is twice the MFPT from the compartment to the narrowest passage in the bottleneck (e.g., the interval \mathbf{AB} in Figure 8). Indeed, the reciprocal of this MFPT is to leading order the rate at which trajectories reach the bottleneck from the first compartment, so the reciprocal of the MFPT is the lowest eigenvalue of the mixed Neumann-Dirichlet boundary value problem in the first compartment with Dirichlet conditions on the cross section of the neck.

There is a spectral gap of order 1 from the smallest eigenvalue to the next one. It follows that long transition times of Brownian trajectories between compartments connected by bottlenecks are exponentially distributed and therefore the leading eigenvalues of Neumann's problem for the Laplace equation in a domain that consists of compartments interconnected by narrow necks are to leading order the eigenvalues of a Markov chain with transition rates that are the reciprocals of the MFPTs through the narrow necks, as is the case for diffusion in a potential landscape with several deep wells (high barriers) [20, 21] (see also [15]). The evaluation of the leading eigenvalues of the Neumann problem for the Laplace equation in domains with bottlenecks reduces to the computation of the leading order eigenvalue for the mixed Neumann-Dirichlet boundary value problem for the Laplace equation in a domain with reflecting (Neumann) boundary except for a small absorbing (Dirichlet) window at the end of a funnel. Some estimates on the asymptotic behavior of the leading eigenvalue are given in [36], [37] and references therein.

5.1 Eigenvalue of the mixed problem in domains with bottlenecks

First we consider the principal eigenvalue of the mixed Neumann-Dirichlet problem for the Laplace equation in a composite domain that consists of a head Ω_1 connected by a funnel to a narrow cylindrical neck Ω_2 . The boundary of the domain is reflecting (Neumann) and only the end of the cylinder $\partial\Omega_a$ is absorbing (Dirichlet). The left half of Figure 8 shows the composite domain and the absorbing boundary is the interval \mathbf{AB} . In the three-dimensional

case the Dirichlet boundary $\partial\Omega_a$ is a small absorbing disk at the end of the cylinder. The domain Ω_1 is the one shown in Figure 2 and it is connected to the cylinder at an interface $\partial\Omega_i$, which in this case is the interval AB in Figure 2. It was shown in [14] that the MFPT from $\mathbf{x} \in \Omega_1$ to $\partial\Omega_a$ is given by

$$\bar{\tau}_{\mathbf{x} \rightarrow \partial\Omega_a} = \bar{\tau}_{\mathbf{x} \rightarrow \partial\Omega_i} + \frac{L^2}{2D} + \frac{|\Omega_1|L}{|\partial\Omega_a|D}. \quad (87)$$

The principal eigenvalue of the mixed two- and three-dimensional Neumann-Dirichlet problems in domains with small Dirichlet and large Neumann parts of a smooth boundary is asymptotically the reciprocal of the MFPT given in (87). Thus the principal eigenvalue λ_1 in a domain with a single bottleneck is given by

$$\lambda_1 \sim \frac{1}{\bar{\tau}_{\mathbf{x} \rightarrow \partial\Omega_i} + \frac{L^2}{2D} + \frac{|\Omega_1|L}{|\partial\Omega_a|D}}, \quad (88)$$

where $\bar{\tau}_{\mathbf{x} \rightarrow \partial\Omega_i}$ is any one of the MFPTs given in (1)-(8), depending on the geometry of Ω_1 .

If a composite domain consists of a single head and N well-separated bottlenecks of different radii and neck lengths, the derivation of (73) shows that the reciprocal of the MFPT is the sum of the reciprocals of the NETs from a domain with a single bottleneck. That is, the principal eigenvalue λ_P is given by

$$\lambda_P \sim \sum_{j=1}^N \lambda_j. \quad (89)$$

This can be interpreted as the fact that the total efflux is the sum of N independent effluxes through the bottlenecks.

5.2 The principal eigenvalue in dumbbell-shaped domains

We consider now the principal eigenvalue of the Neumann problem in a dumbbell-shaped domain that consists of two compartments Ω_1 and Ω_3 and a connecting neck Ω_2 that is effectively one-dimensional, such as shown in Figure 8, or in a similar domain with a long neck. We assume, as we may, that the stochastic separatrix (SS) in the neck is the cross section at its center. In the planar case it is the segment \mathbf{AB} in Figure 8. This means that a Brownian trajectory that hits the SS is equally likely to reach either compartment before the other. Thus the mean time to traverse the neck from compartment Ω_1 to compartment Ω_3 is asymptotically twice the MFPT $\bar{\tau}_{\mathbf{x} \rightarrow SS}$ from $\mathbf{x} \in \Omega_1$ to the SS [18]. This MFPT is to leading order independent of $\mathbf{x} \in \Omega_1$ and can be denoted $\bar{\tau}_{\Omega_1 \rightarrow SS}$.

First, we note that the mean residence time of a Brownian trajectory in Ω_1 or in Ω_3 is much larger than that in Ω_2 when the neck is narrow. Second, we note that the first passage time $\tau_{\mathbf{x} \rightarrow SS}$ for $\mathbf{x} \in \Omega_1$ is exponentially distributed for long times and so is $\tau_{\mathbf{x} \rightarrow SS}$ for $\mathbf{x} \in \Omega_3$ [22]. We can therefore coarse-grain the Brownian motion to a two-state Markov process (a telegraph process), which is in State I when the Brownian trajectory is in Ω_1 and is State

II when it is in Ω_3 . The state Ω_2 and the residence time there can be neglected relative to those in Ω_1 and Ω_3 . The transition rates from I to II and from II to I are, respectively,

$$\lambda_{I \rightarrow II} = \frac{1}{2\bar{\tau}_{\Omega_1 \rightarrow SS}}, \quad \lambda_{II \rightarrow I} = \frac{1}{2\bar{\tau}_{\Omega_3 \rightarrow SS}}. \quad (90)$$

These rates can be found from (88), with L half the length of the neck and $SS = \partial\Omega_a$. The radii of curvature $R_{c,1}$ and $R_{c,3}$ at the two funnels may be different, and the domain is either Ω_1 or Ω_3 , as the case may be. The smallest positive eigenvalue λ of the Neumann problem for the Laplace equation in the dumbbell is to leading order that of the two-state Markov process, which is $\lambda = -(\lambda_{I \rightarrow II} + \lambda_{II \rightarrow I})$ (see Appendix below). For example, if the solid dumbbell consists of two general heads connected smoothly to the neck by funnels (see (4)), the two rates are given by

$$\frac{1}{\lambda_{I \rightarrow II}} = \sqrt{2} \left[\left(\frac{R_{c,1}}{a} \right)^{3/2} \frac{|\Omega_1|}{R_{c,1}D} \right] (1 + o(1)) + \frac{L^2}{4D} + \frac{|\Omega_1|L}{\pi a^2 D} \quad (91)$$

$$\frac{1}{\lambda_{II \rightarrow I}} = \sqrt{2} \left[\left(\frac{R_{c,3}}{a} \right)^{3/2} \frac{|\Omega_3|}{R_{c,3}D} \right] (1 + o(1)) + \frac{L^2}{4D} + \frac{|\Omega_3|L}{\pi a^2 D}. \quad (92)$$

Next, we consider the Neumann problem for the Laplace equation in a domain that consists of any number of heads interconnected by narrow necks. The Brownian motion can be coarse-grained into a Markovian random walk that jumps between the connected domains at exponentially distributed times with rates determined by the first passage times and exit probabilities, as described in Section 5.1. This random walk can in turn be approximated by an effective coarse-grained anisotropic diffusion, as done, for example, for atomic migration in crystals [38, Ch.8, Sect. 2] and for effective diffusion on a surface with obstacles [15].

6 A Brownian needle in dire straits

As an application of the methodology described above, we study the planar diffusion of a stiff thin rod (needle) of length l in an infinite horizontal strip of width $l_0 > l$. We assume that the rod is a long thin right circular cylinder with radius $\epsilon \ll l_0$ (Figure 9). The planar motion of the rod is described by two coordinates of the centroid and the rotational angle θ between the axes of the strip and the rod. The y -coordinate of the center of the rod is measured from the axis of the strip. The motion of the rod is confined to the domain Ω shown in Figure 9b. The rod turns across the vertical position if it goes from the green to the blue domains or in the reverse direction. If

$$\epsilon = \frac{l_0 - l}{l_0} \ll 1, \quad (93)$$

the black window becomes narrow and the mean first passage times (MFPT) $\tau_{\text{Green} \rightarrow \text{Black}}$ and $\tau_{\text{Blue} \rightarrow \text{Black}}$, from the green or blue to the black segment, become much longer than those in the other directions. The former also become independent of the starting position outside a

boundary layer near the black segment. Thus the definition of the time to turn is independent of the choice of the green and blue domains, as long as they are well separated from the black segment. The neck near the black domain is the boundary layer region near $\theta = \pi/2$. We neglect henceforward the short times relative to the long ones.

To turn across the vertical position the rod has to reach the black domain from the green one for the first time and then to reach the blue domain for the first time, having returned to the green domain any number of times prior to reaching the blue domain. Due to symmetry, a simple renewal argument shows that the mean time to turn, $\tau_{\text{Blue} \rightarrow \text{Green}}$, is asymptotically given by

$$\tau_{\text{Blue} \rightarrow \text{Green}} \sim 2\tau_{\text{Blue} \rightarrow \text{Black}} \quad \text{for} \quad \frac{l_0 - l}{l_0} \ll 1. \quad (94)$$

The time to turn is invariant to translations along the strip (the x -axis), therefore it suffices to describe the rod movement by its angle θ and the y coordinate of its center. The position of the rod is defined for $\theta \bmod \pi$. Therefore the motion of the rod in the invariant strip can be mapped into that in the (θ, y) planar domain Ω (see Fig.9b):

$$\Omega = \left\{ (\theta, y) : |y| < \frac{l_0 - l \sin \theta}{2}, \quad 0 < \theta < \pi \right\}. \quad (95)$$

6.1 The diffusion law of a Brownian needle in a planar strip

In a rotating system of coordinates (X, Y, θ) , where the instantaneous X -axis is parallel to the long axis of the rod and the Y -axis is perpendicular to it, the diffusive motion of the rod is an anisotropic Brownian motion, and can be described by the stochastic equations

$$\dot{X} = \sqrt{2D_X} \dot{w}_1$$

$$\dot{Y} = \sqrt{2D_Y} \dot{w}_2$$

$$\dot{\theta} = \sqrt{2D_r} \dot{w}_3,$$

where D_X is the longitudinal diffusion coefficient along the axis, D_Y the transversal diffusion constant and D_r , the rotational diffusion coefficient. Due to the anisotropy, the rod makes in general larger excursions in the X -direction than in the Y -direction and this usually characterized by the ratio $\frac{D_Y}{D_X}$. In a fixed system of Cartesian coordinates (x, y) , the translational and rotational motion of the centroid $(x(t), y(t))$ and the angle of rotation $\theta(t)$ of the rod is governed by the Itô equations

$$\dot{x} = \cos(\theta) \sqrt{2D_X} \dot{w}_1 - \sin(\theta) \sqrt{2D_Y} \dot{w}_2$$

$$\dot{y} = \sin(\theta) \sqrt{2D_X} \dot{w}_1 + \cos(\theta) \sqrt{2D_Y} \dot{w}_2$$

$$\dot{\theta} = \sqrt{2D_r} \dot{w}_3,$$

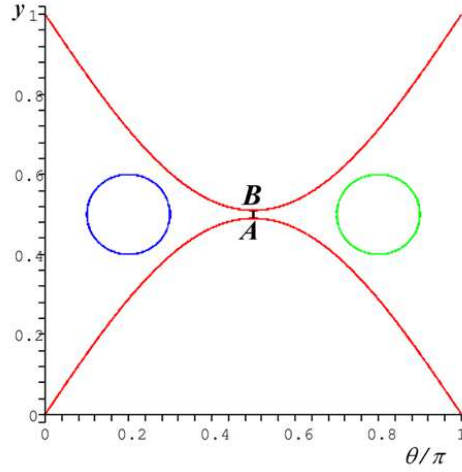
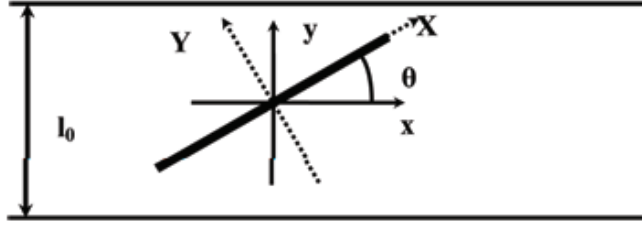


Figure 9: **Top:** Rod in strip . The strip width is l_0 and the rod length is $l < l_0$. The position of the rod is characterized by the angle θ and the fixed coordinates x and y and the rotating system of coordinates (X, Y, θ) . **Bottom:** The motion of the rod is confined to the domain Ω in the y, θ plane.

which can be put in the matrix form

$$\dot{\mathbf{x}}(t) = \mathbf{B}(\theta) \dot{\mathbf{w}},$$

where

$$\mathbf{x} = \begin{pmatrix} x \\ y \\ \theta \end{pmatrix}, \quad \mathbf{w} = \begin{pmatrix} w_1 \\ w_2 \\ w_3 \end{pmatrix}$$

and

$$\mathbf{B}(\theta) = \sqrt{2} \begin{pmatrix} \cos \theta & -\sin \theta & 0 \\ \sin \theta & \cos \theta & 0 \\ 0 & 0 & 1 \end{pmatrix} \begin{pmatrix} \sqrt{D_X} & 0 & 0 \\ 0 & \sqrt{D_Y} & 0 \\ 0 & 0 & \sqrt{D_r} \end{pmatrix}.$$

The probability density function of the rod in the product space $\Omega \times \mathbb{R}$,

$$p(t, x, y, \theta) d\mathbf{x} = \Pr\{(x(t), y(t), \theta(t)) \in \mathbf{x} + d\mathbf{x}\}, \quad (96)$$

satisfies the Fokker-Planck equation

$$\frac{\partial p(t, \mathbf{x})}{\partial t} = -\nabla \cdot \mathbf{J}(t, \mathbf{x}),$$

where the flux is given by

$$\mathbf{J}(t, \mathbf{x}) = - \begin{pmatrix} [D_X \cos^2 \theta + D_Y \sin^2 \theta] \frac{\partial p}{\partial x} + \frac{1}{2} [(D_X - D_Y) \sin 2\theta] \frac{\partial p}{\partial y} \\ [D_X \sin^2 \theta + D_Y \cos^2 \theta] \frac{\partial p}{\partial y} + \frac{1}{2} [(D_X - D_Y) \sin 2\theta] \frac{\partial p}{\partial x} \\ D_r \frac{\partial p}{\partial \theta} \end{pmatrix}. \quad (97)$$

The boundary conditions are π -periodic in θ , because the position of the rod is defined modulo π (note that $\mathbf{J}(t, \mathbf{x})$ is π -periodic in θ). This means that the density $p(t, x, y, \theta)$ is π -periodic and the normal flux $-D_r \partial p(t, x, y, \theta) / \partial \theta$ is π -antiperiodic in θ .

The MFPT $\tau_{\text{Blue} \rightarrow \text{Black}}$ is translation-invariant with respect to x and is, therefore, the solution $u(\theta, y)$ of the boundary value problem

$$D_r \frac{\partial^2 u(\theta, y)}{\partial \theta^2} + D_y(\theta) \frac{\partial^2 u(\theta, y)}{\partial y^2} = -1 \quad \text{for } (\theta, y) \in \Omega_1, \quad (98)$$

where $D_y(\theta) = D_X \sin^2 \theta + D_Y \cos^2 \theta$ and $\Omega_1 = \Omega \cap \left\{ \theta < \frac{\pi}{2} \right\}$, with the boundary conditions

$$\frac{\partial u}{\partial \tilde{\mathbf{n}}} = 0 \quad \text{for } (\theta, y) \text{ on the red boundary and at } \theta = 0 \quad (99)$$

$$u\left(\frac{\pi}{2}, y\right) = 0 \quad \text{for } |y| < l_0 - l, \quad (100)$$

where the co-normal derivative of $u(\theta, y)$ on the red boundary is given by

$$\frac{\partial u}{\partial \tilde{\mathbf{n}}} = \nabla u(\theta, y) \cdot \tilde{\mathbf{n}}(\theta) \quad \text{for } (\theta, y) \text{ on the red boundary} \quad (101)$$

and the co-normal vector $\tilde{\mathbf{n}}(\theta)$ is given by

$$\tilde{\mathbf{n}}(\theta) = \begin{pmatrix} D_r & 0 \\ 0 & D_y(\theta) \end{pmatrix} \mathbf{n}(\theta) \quad (102)$$

with $\mathbf{n}(\theta)$ – the unit normal vector to the red boundary.

Introducing the dimensionless variables

$$X' = \frac{X}{l_0}, \quad Y' = \frac{Y}{l_0}, \quad \xi(t) = \frac{x(t)}{l_0}, \quad \eta(t) = \frac{y(t)}{l_0}$$

and the normalized diffusion coefficients

$$D'_X = \frac{D_X}{l_0^2}, \quad D'_Y = \frac{D_Y}{l_0^2}, \quad D_\eta(\theta) = \frac{D_y(\theta)}{l_0^2},$$

we find that the domain Ω in (95) is mapped into

$$\Omega' = \left\{ (\theta, \eta) : |\eta| < \frac{1 - (1 - \varepsilon) \sin \theta}{2}, \quad 0 < \theta < \pi \right\}. \quad (103)$$

To convert (98) to canonical form, we introduce the variable

$$\varphi(\theta) = \int_0^\theta \sqrt{\frac{D_\eta(\theta')}{D_r}} d\theta', \quad (104)$$

which defines the inverse function $\theta = \theta(\varphi)$, and set $u(\theta, y) = U(\varphi, \eta)$ to obtain

$$U_{\varphi\varphi}(\varphi, \eta) + U_{\eta\eta}(\varphi, \eta) = U_\varphi(\varphi, \eta) \sqrt{D_r} \frac{dD_\eta^{-1/2}(\theta)}{d\theta} - \frac{1}{D_\eta(\theta)}. \quad (105)$$

The domain Ω' , defined in (103), is mapped into the similar domain

$$\Omega'' = \left\{ (\varphi, \eta) : |\eta| < \frac{1 - (1 - \varepsilon) \sin \theta(\varphi)}{2}, \quad 0 < \varphi < \varphi(\pi) \right\} \quad (106)$$

in the (φ, η) plane. Because the the co-normal direction at the boundary becomes normal, so does the co-normal derivative. It follows that the no-flux boundary condition (99) and the absorbing condition (100) become

$$\begin{aligned} \frac{\partial U(\varphi, \eta)}{\partial n} &= 0 \text{ for } (\theta(\varphi), \eta) \text{ on } \partial\Omega'' \text{ (the red boundary in the scaled Figure 9b)} \\ \frac{\partial U(0, \eta)}{\partial \varphi} &= 0 \text{ for } |\eta| < \frac{1}{2} \\ U\left(\varphi\left(\frac{\pi}{2}\right), \eta\right) &= 0 \text{ for } |\eta| < \frac{\varepsilon}{2}, \end{aligned} \quad (107)$$

respectively. The gap at $\theta = \pi/2$ is preserved and the (dimensionless) radius of curvature of the boundary at the gap is

$$R' = \frac{2D_\eta\left(\frac{\pi}{2}\right)}{(1 - \varepsilon)D_r} = \frac{2D_X}{(1 - \varepsilon)l_0^2 D_r}. \quad (108)$$

First, we simplify (105) by setting

$$g(\varphi) = \sqrt{D_r} \frac{dD_\eta^{-1/2}(\theta)}{d\theta}, \quad U(\varphi, \eta) = f(\varphi)V(\varphi, \eta) \quad (109)$$

and choosing $f(\varphi)$ such that $f'(\varphi) = \frac{1}{2}f(\varphi)g(\varphi)$. Note that

$$\left. \frac{dD_\eta^{-1/2}(\theta)}{d\theta} \right|_{\theta=0, \pi/2, \pi} = 0. \quad (110)$$

Equation (105) becomes

$$V_{\varphi\varphi} + V_{\eta\eta} = \frac{1}{f(\varphi)} \left\{ [g(\varphi)f'(\varphi) - f''(\varphi)]V - \frac{1}{D_\eta(\theta(\varphi))} \right\}. \quad (111)$$

Next, we move the origin to the center of curvature of the lower boundary by setting

$$\zeta = -\left(\eta - R' - \frac{\varepsilon}{2}\right) + i\left[\varphi - \varphi\left(\frac{\pi}{2}\right)\right]$$

and use the conformal mapping (16),

$$\omega = \frac{\zeta - R'\alpha}{R' - \alpha\zeta}, \quad (112)$$

with $\omega = \rho e^{i\psi}$. We also have

$$w'(\zeta) = \frac{1}{R'} \frac{(1 + \alpha w)^2}{1 - \alpha^2} \quad (113)$$

$$|w'(\zeta)|^2 = \frac{1}{R'^2} \left| \frac{(1 + \alpha w)^2}{1 - \alpha^2} \right|^2 = \frac{|1 - w + \sqrt{\varepsilon}w|^4}{4\varepsilon R'^2} (1 + O(\sqrt{\varepsilon})), \quad (114)$$

The image Ω_ω of the domain Ω is given in Figure 10 and is similar to Ω_w in Figure 5, except

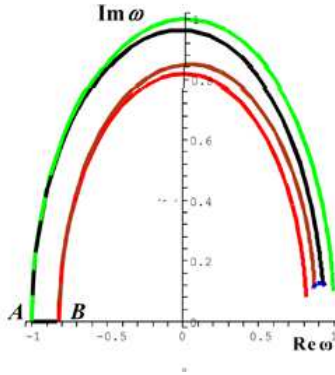


Figure 10: The image Ω_ω of the domain Ω under the mapping (112). The values of the parameters are $\varepsilon = 0.01$ with the approximation $D_Y \ll D_X$. The domain is enclosed by the real segment AB and by the brown, black, and blue curves. The green and red curves are the images of arcs of the osculating circles at the narrow neck, as in Figure 5.

for a small distortion near $\psi = c\sqrt{\varepsilon}$, which we neglect, as we may. Setting $V(\varphi, \eta) = W(\rho, \psi)$,

fixing $\rho = 1$ in Ω_ω , as in Section 2, and abbreviating $W = W(\psi, 1)$, equation (111) becomes to leading order

$$W_{\psi\psi} + \frac{h(\psi)}{|\omega'(\zeta)|^2} W = -\frac{1}{|\omega'(\zeta)|^2 k(\psi)}, \quad (115)$$

where

$$h(\psi) = \left. \frac{f''(\varphi) - g(\varphi)f'(\varphi)}{f(\varphi)} \right|_{\rho=1}, \quad k(\psi) = f(\varphi)D_\eta(\theta(\varphi))|_{\rho=1}. \quad (116)$$

Using (18) and neglecting terms of order $O(\varepsilon)$, we rewrite (115) as

$$W_{\psi\psi} + \frac{4\varepsilon R^2 h(\psi)}{|e^{i\psi}(1 - \sqrt{\varepsilon}) - 1|^4} W = -\frac{4\varepsilon R^2}{|e^{i\psi}(1 - \sqrt{\varepsilon}) - 1|^4 k(\psi)}. \quad (117)$$

In view of (110), the boundary conditions (107) become

$$W_\psi(c\sqrt{\varepsilon}) = 0, \quad W(\pi) = 0. \quad (118)$$

6.2 The asymptotic solution

The construction of the asymptotic expansion of the solution of the boundary layer equation (117) is similar to that in Section 3.1. The outer solution of (117) is a linear function $W_{\text{outer}}(\psi) = a\psi + b$, where a and b are yet undetermined constants. The uniform approximation is constructed as $W_{\text{uniform}}(\psi) = W_{\text{outer}}(\psi) + W_{\text{bl}}(\psi)$, where the boundary layer $W_{\text{bl}}(\psi)$ is a function $Y(\xi)$ of the boundary layer variable $\xi = \psi/\sqrt{\varepsilon}$. The boundary layer equation is

$$Y''(\xi) + \frac{4R^2 h(0)}{(1 + \xi^2)^2} Y(\xi) = -\frac{4R^2}{(1 + \xi^2)^2 k(0)}, \quad (119)$$

which is simplified by the substitution $Y(\xi) = \tilde{Y}(\xi) + 1/h(0)k(0)$ to

$$\tilde{Y}''(\xi) + \frac{4R^2 h(0)}{(1 + \xi^2)^2} \tilde{Y}(\xi) = 0. \quad (120)$$

The boundary conditions (118) become $\tilde{Y}'(c) = 0$ and $\tilde{Y}(\infty) = 1/h(0)k(0)$. The boundary layer equation (120) has two linearly independent solutions, $\tilde{Y}_1(\xi)$ and $\tilde{Y}_2(\xi)$, which are linear for sufficiently large ξ . Initial conditions for $\tilde{Y}_1(\xi)$ and $\tilde{Y}_2(\xi)$ can be chosen so that $\tilde{Y}_2(\xi) \rightarrow \text{const}$ as $\xi \rightarrow \infty$ (e.g., $\tilde{Y}_2(0) = -4.7$, $\tilde{Y}_2'(0) = -1$, see Figure 6). Thus the boundary layer function is given by

$$W_{\text{bl}}(\psi) = A\tilde{Y}_1\left(\frac{\psi}{\sqrt{\varepsilon}}\right) + B\tilde{Y}_2\left(\frac{\psi}{\sqrt{\varepsilon}}\right) + C, \quad (121)$$

where A and B are constants to be determined and C is related to the constant $1/h(0)k(0)$ and is also determined below from the boundary and matching conditions.

The matching condition is that $W_{\text{bl}}(\psi) = A\tilde{Y}_1(\psi/\sqrt{\varepsilon}) + B\tilde{Y}_2(\psi/\sqrt{\varepsilon}) + C$ remains bounded as $\xi \rightarrow \infty$, which implies $A = 0$. It follows that at the absorbing boundary $\psi = \pi$ we have

$$\begin{aligned} W_{\text{unif}}(\pi) &= a\pi + b' = 0 \\ W'_{\text{unif}}(\pi) &= a. \end{aligned} \quad (122)$$

where the constant b' incorporates all remaining constants. At the reflecting boundary we have to leading order

$$W'_{\text{unif}}(c\sqrt{\varepsilon}) = W'_{\text{outer}}(c\sqrt{\varepsilon}) + W'_{\text{bl}}(c\sqrt{\varepsilon}) = a + B\frac{\tilde{Y}'_2(c)}{\sqrt{\varepsilon}} = 0, \quad (123)$$

which gives

$$B = -\frac{a\sqrt{\varepsilon}}{\tilde{Y}'_2(c)}, \quad b' = -a\pi. \quad (124)$$

The uniform approximation to $W(\omega)$ is given by

$$W_{\text{unif}}(\rho e^{i\psi}) = a \left(\psi - \pi - \frac{\sqrt{\varepsilon}}{\tilde{Y}'_2(c)} \right), \quad (125)$$

so that using (109), (110), and (113), we obtain from (125)

$$\frac{\partial u}{\partial n} \Big|_{\zeta \in \partial\Omega_a} = f\left(\varphi\left(\frac{\pi}{2}\right)\right) \frac{\partial W(\rho e^{i\psi})}{\partial \psi} \Big|_{\psi=\pi} \omega'(\zeta) \Big|_{\zeta=-1} \frac{\partial \varphi}{\partial \theta} \Big|_{\theta=\pi/2} = a\sqrt{\frac{2}{\varepsilon R'}}(1 + O(\sqrt{\varepsilon})). \quad (126)$$

Because $W(\omega)$ scales with $1/f(\varphi)$ relative to $V(\varphi, \eta)$, we may choose at the outset $f(\varphi(\pi/2)) = 1$.

Finally, to determine the value of a , we integrate (98) over Ω , use (126), and the fact that

$$\int_{\partial\Omega_a} dy = l_0\varepsilon,$$

to obtain $a = -|\Omega|\sqrt{R'}/l_0D_r\sqrt{2\varepsilon}$. Now (125) gives the MFPT at any point \mathbf{x} in the head as

$$E[\tau | \mathbf{x}] = u(\mathbf{x}) \sim W\left(\rho e^{ic\sqrt{\varepsilon}}\right) \sim -a\pi = \frac{\pi|\Omega|\sqrt{R'}}{l_0D_r\sqrt{2\varepsilon}}(1 + O(\sqrt{\varepsilon})) \text{ for } \varepsilon \ll 1. \quad (127)$$

Reverting to the original dimensional variables, we get

$$E[\tau | \mathbf{x}] = \frac{\pi\left(\frac{\pi}{2} - 1\right)}{D_r\sqrt{l_0(l_0 - l)}} \sqrt{\frac{D_X}{D_r}} \left(1 + O\left(\sqrt{\frac{l_0 - l}{l_0}}\right) \right), \quad (128)$$

which is (10).

7 Discussion and conclusion

This paper develops a boundary layer theory for the solution of the mixed Neumann-Dirichlet problem for the Poisson equation in geometries in which the methodologies of [1]-[12] fail. These methodologies were used for the narrow escape problem. In the geometries considered here the small Dirichlet part is located at the end of narrow straits connected smoothly to the Neumann boundary of the domain. Additional problems related to Brownian motion in composite domains that contain a cylindrical narrow neck connected smoothly or sharply to the head are considered in [14]. These include the asymptotic evaluation of the NET, of the leading eigenvalue in dumbbell-shaped domains and domains with many heads interconnected by narrow necks, the escape probability through any one of several narrow necks, and more.

Our results have applications in several areas. The first application is in neuroscience and concerns dendritic spines, which are believed to be the locus of postsynaptic transmission. Recognized more than 100 years ago by Ramón y Cajal, dendritic spines are small terminal protrusions on neuronal dendrites, and are the postsynaptic parts of excitatory synaptic connections. The spine consists of a relatively narrow cylindrical neck connected to a bulky head. The geometrical shape of a spine correlates with its physiological function [29]-[33]. Several physiological phenomena are regulated by diffusion in dendritic spines. For example, synaptic plasticity is induced by the transient increase of calcium concentration in the spine, which is regulated by spine geometry, by endogenous buffers, and by the number and rates of exchangers [31, 34, 35, 23, 24]. Another significant function of the spine is the regulation of the number and type of receptors that contribute to the shaping of the synaptic current [25]-[28]. Indeed, the neurotransmitter receptors, such as AMPA and NMDA, whose motion on the spine surface is diffusion, mediate the glutamatergic-induced synaptic current. Thus dendritic spines regulate both two-dimensional motion of neurotransmitter receptors on its surface, and the three-dimensional diffusive motion of ions (e.g., calcium), molecules, proteins (e.g., mRNA), or small vesicles in the bulk. Our results give a quantitative measure of the effect of geometry on regulation of flux.

In a biochemical context, the NET (eq. 69) accounts for the local geometry near an active binding site occluded by the molecular structure of the protein. This is the case of proton binding sites located on spike proteins, located on the viral envelope of the influenza virus and involved in membrane fusion [39]. Another application is that of the turnaround time of Brownian needle. Our result in Section 6 provides the precise time scale of the unraveling of a double strand DNA break confined between two-dimensional membranes [40]. The common feature of the geometries studied in this paper is the cusp-shaped narrow passage leading to the absorbing boundary. The main biological conclusion of our results is that this geometry is the main controller of the flux through biological narrow passages, an effect that is ubiquitous in biological systems. More specific applications of the NET from composite domains to dendritic spines are given in [14].

8 Appendix

The asymmetric random telegraph process jumps between two states, a and b , at independent exponentially distributed waiting times with rates $\lambda_{a \rightarrow b}$ and $\lambda_{b \rightarrow a}$, respectively. The transition probability distribution function satisfies the linear differential equations (see http://en.wikipedia.org/wiki/Telegraph_process, [22])

$$\frac{\partial P\{a, t | x, t_0\}}{\partial t} = -\lambda_{a \rightarrow b}P\{a, t | x, t_0\} + \lambda_{b \rightarrow a}P\{b, t | x, t_0\} \quad (129)$$

$$\frac{\partial P\{b, t | x, t_0\}}{\partial t} = \lambda_{a \rightarrow b}P\{a, t | x, t_0\} - \lambda_{b \rightarrow a}P\{b, t | x, t_0\},$$

which can be written in the obvious matrix notation as $\dot{\mathbf{p}} = \mathbf{A}\mathbf{p}$ with

$$\mathbf{A} = \begin{pmatrix} -\lambda_{a \rightarrow b} & \lambda_{b \rightarrow a} \\ \lambda_{a \rightarrow b} & -\lambda_{b \rightarrow a} \end{pmatrix}.$$

The eigenvalues of \mathbf{A} are 0 with the normalized eigenvector $(\frac{1}{2}, \frac{1}{2})^T$, and $-(\lambda_{a \rightarrow b} + \lambda_{b \rightarrow a})$ with the eigenvector $(1, -1)^T$. It follows that the nonzero eigenvalue of the system (129) is $\lambda = \lambda_{a \rightarrow b} + \lambda_{b \rightarrow a}$.

Acknowledgment: The authors wish to thank F. Marchesoni for pointing out the factor 1/2 in eq.(3).

References

- [1] Ward, M.J. and J.B. Keller, "Strong Localized Perturbations of Eigenvalue Problems", *SIAM J. Appl. Math.* **53**, pp.770–798 (1993).
- [2] Ward, M.J., W.D. Henshaw and J.B. Keller, "Summing Logarithmic Expansions for Singularly Perturbed Eigenvalue Problems", *SIAM J. Appl. Math.*, **53**, pp.799–828 (1993).
- [3] Ward, M.J. and E. Van De Velde, "The Onset of Thermal Runaway in Partially Insulated or Cooled Reactors", *IMA J. Appl. Math.*, **48**, pp.53–85 (1992).
- [4] Kolokolnikov, T., M. Titcombe and M.J. Ward, "Optimizing the Fundamental Neumann Eigenvalue for the Laplacian in a Domain with Small Traps", *European J. Appl. Math.* **16**, pp.161–200 (2005).
- [5] Holcman, D. and Z. Schuss, "Escape through a small opening: receptor trafficking in a synaptic membrane", *J. of Statistical Physics* **117** (5/6), pp.191-230 (2004).
- [6] Singer, A., Z. Schuss, D. Holcman, B. Eisenberg, "Narrow Escape I", *J. Stat. Phys.* **122** (3), pp.437–463 (2006).

- [7] Singer, A., Z. Schuss, D. Holcman, "Narrow Escape II", *J. Stat. Phys.* **122** (3), pp.465–489 (2006)
- [8] Singer, A., Z. Schuss, D. Holcman, "Narrow Escape III", **122** (3), pp.491-509, (2006).
- [9] A. Gandolfi, A. Gerardi, and F. Marchetti. "Diffusion-Controlled Reactions in Two Dimensions" *Acta Applicandae Mathematicae* **4**, pp.139–159 (1985).
- [10] Linderman, J. and D. Lauffenberger. "Analysis of intracellular receptor/Ligand sorting: calculation of mean surface and bulk diffusion times within a sphere". *Biophys. J.* **50**, pp.295–305 (1986).
- [11] Coombs, D., R. Straube, and M. Ward. "Diffusion on a Sphere with Localized Traps: Mean First Passage Time, Eigenvalue Asymptotics, and Fekete Points." *SIAM J. Appl. Math.* **70** (1), pp.302-332 (2009).
- [12] Schuss, Z., A. Singer, D. Holcman. "The narrow escape problem for diffusion in cellular microdomains." *Proc. Natl. Acad. Sci. USA* ;104(41):16098-103 (2007).
- [13] I. V. Grigoriev, Y. A. Makhnovskii, A. M. Berezhkovskii, V. Y. Zitserman, "Kinetics of escape through a small hole", *J. Chem. Phys.*, **116** (22), pp.9574-9577 (2002).
- [14] Holcman, D. and Z. Schuss. "Diffusion laws in dendritic spines." *The Journal of Mathematical Neuroscience* **1**, p.10 (2011) doi:10.1186/2190-8567-1-10.
- [15] Holcman, D., N. Hoze, Z. Schuss. "Narrow escape through a funnel and effective diffusion on a crowded membrane." *Phys. Rev. E* **84**:021906 (2011).
- [16] Singer, A., Z. Schuss and D. Holcman. "Narrow escape and leakage of Brownian particles." *Physical Review E* **78**, 051111 (2008).
- [17] Cheviakov, A., M.J. Ward, and R. Straube. "An Asymptotic Analysis of the Mean First Passage Time for Narrow Escape Problems: Part II: The Sphere." *SIAM Multiscale Modeling and Simulation* **8** (3), pp. 836–870, (2010).
- [18] Z. Schuss. "Equilibrium and Recrossings of the Transition State: What Can Be Learned from Diffusion?" *J. Phys. Chem. C*, **114** (48), 20320–20334 (2010).
- [19] Jackson, J. *Classical Electrodynamics*. Wiley, New York, 3rd ed. 1998 pp. 27–35.
- [20] Matkowsky, B.J. and Z. Schuss. "Eigenvalues of the Fokker-Planck operator and the approach to equilibrium in potential fields", *SIAM J. Appl. Math.* **40**, pp.242-252, (1981).
- [21] Hänggi, P., P. Talkner and M. Borkovec, "Reaction-rate theory: Fifty years after Kramers." *Rev. Mod. Phys.* **62**, pp.251-332 (1990).
- [22] Schuss, Z. *Diffusion and Stochastic Processes: an Analytical Approach*. Springer NY, 2010.

- [23] Biess, A., E. Korkotian, D. Holcman. "Diffusion in a dendritic spine: the role of geometry." *Phys. Rev. E Stat. Nonlin. Soft Matter Phys.* 021922 (2007).
- [24] Holcman, D., I. Kupka. "Some questions in computational cellular biology." *Journal of Fixed Point Theory and Applications* **7** (1):67-83 (2010), DOI: 10.1007/s11784-010-0012-1.
- [25] Borgdorff, A.J., D. Choquet. "Regulation of AMPA receptor lateral movements." *Nature* **417** (6889):649-53 (2002).
- [26] Choquet, D., A. Triller. "The role of receptor diffusion in the organization of the post-synaptic membrane." *Nat. Rev. Neurosci.* **4**:251-65 (2003).
- [27] Holcman, D., A. Triller. "Modeling synaptic dynamics and receptor trafficking." *Biophys. J.* **91** (7):2405-15 (2006).
- [28] Holcman, D., E. Korkotian, M. Segal. "Calcium dynamics in dendritic spines, modeling and experiments." *Cell Calcium* **37** (5):467-75 (2005).
- [29] Harris, K.M., J.K. Stevens. "Dendritic spines of rat cerebellar Purkinje cells: serial electron microscopy with reference to their biophysical characteristics." *J. Neurosci.* **12**:4455-69 (1988).
- [30] Bourne, J.N., K.M. Harris. "Balancing Structure and Function at Hippocampal Dendritic Spines." *Annu. Rev. Neurosci.* **31**: 47-67 (2008).
- [31] Korkotian, E., D. Holcman, M. Segal. "Dynamic Regulation of Spine-Dendrite Coupling in Cultured Hippocampal Neurons," *Euro. J. of Neuroscience*, **20** (10), pp.2649-63 (2004).
- [32] Hotulainen, P., C.C. Hoogenraad. "Actin in dendritic spines: connecting dynamics to function." *J. Cell Biol.* **189** (4):619-29 (2010).
- [33] Newpher, T.M., M.D. Ehlers. "Spine microdomains for postsynaptic signaling and plasticity." *Trends Cell Biol.* **5**:218-27 (2009).
- [34] Yuste, R., A. Majewska, K. Holthoff. "From form to function: calcium compartmentalization in dendritic spines." *Nat. Neurosci.* **7**:653-9 (2000).
- [35] Svoboda, K., D.W. Tank, W. Denk. "Direct measurement of coupling between dendritic spines and shafts." *Science* **272** (5262):716-9 (1996).
- [36] Arrieta, J.M. "Rates of Eigenvalues on a Dumbbell Domain. Simple Eigenvalue Case." *Trans. AMS* **347** (9), pp.3503-3531 (1995).
- [37] Ward, M.J. and D. Stafford. "Metastable dynamics and spatially inhomogeneous equilibria in dumbbell-shaped domains." *Stud. Appl. Math.* **103** (1), pp.51-73 (1999).
- [38] Schuss, Z. *Theory and Applications of Stochastic Differential Equations*. John Wiley, New York, 1980.

- [39] Huang Q, Opitz R, Knapp EW, Herrmann A., Protonation and stability of the globular domain of influenza virus hemagglutinin. *Biophys J.* 2002 Feb;82(2):1050-8.
- [40] Lieber A, Leis A, Kushmaro A, Minsky A, Medalia O., Chromatin organization and radio resistance in the bacterium *Gemmata obscuriglobus*. *J Bacteriol. J Bacteriol.*;191(5):1439-45. (2009)